

Letter

An Acridine-Based Fluorescent Sensor for Monitoring ClO^- in Water Samples and Zebrafish

Su Chan Lee ¹, Soyoung Park ¹, Haeri So ¹, Gyudong Lee ², Ki-Tae Kim ^{2,*} and Cheal Kim ^{1,*}

¹ Department of Fine Chemistry, Seoul National University of Science and Technology, Seoul 136-741, Korea; rlthro456@naver.com (S.C.L.); pp113833@hanmail.net (S.P.); gofl0988@naver.com (H.S.)

² Department of Environmental Engineering, Seoul National University of Science and Technology, Seoul 136-741, Korea; rbehd8024@gmail.com

* Correspondence: ktkim@snut.ac.kr (K.-T.K.); chealkim@snut.ac.kr (C.K.); Tel.: +82-2-960-6683 (K.-T.K. & C.K.); Fax: +82-2-971-9139 (C.K.)

Received: 30 July 2020; Accepted: 20 August 2020; Published: 23 August 2020



Abstract: A novel acridine-based fluorescent chemosensor, **BK** ((E)-2-((acridine-9-ylimino)methyl)-N-benzhydrylhydrazine-1-carbothioamide), for monitoring ClO^- was prepared. The sensor **BK** was synthesized by introducing a new synthetic route of making aldehyde group using formic hydrazide. Probe **BK** displayed notable fluorescence quenching in the presence of ClO^- and showed a great selectivity over other guest analytes. The detection limit was calculated to be 7.65 μM . Additionally, **BK** was satisfactorily applied for sensing ClO^- in water samples and zebrafish.

Keywords: acridine; fluorescent chemosensor; hypochlorite; zebrafish; theoretical calculations

1. Introduction

Interest in quantification of reactive oxygen species (ROS) has grown owing to the indispensable role played by ROS in pathological and physiological processes [1–5]. For instance, recent research revealed that cancer cells steadily produce high concentrations of intracellular ROS, owing to carcinogenic deformation [6–8]. Hypochlorite (ClO^-) is one of the ROS, which was produced from the oxidation reaction of Cl^- and H_2O_2 catalyzed by the heme protein myeloperoxidase [9–11]. Hypochlorite is well known as a bactericidal agent because of the capability to kill the deleterious bacteria and pathogens [12–15]. However, the abnormal levels of ClO^- in life systems are related to various diseases like cystic fibrosis, neuron degeneration, kidney disease, arthritis, atherosclerosis, and cancer [16–20]. Hence, there is urgent need to develop effective and dependable sensors for detecting ClO^- to understand the role of hypochlorite in organisms.

Until now, various analytical methods for the sensing of ClO^- have been established, such as electrochemistry, colorimetry assays, spectrophotometry and fluorescent chemosensors [21–24]. Among the methods for detecting ClO^- , fluorescence imaging techniques have various virtues like specificity, superior sensitivity, manageability and fast response times [25–28]. Hitherto, several probes having fluorophores have been developed for sensing ClO^- like 1,8-diaminonaphthalene, phenanthrene, BODIPY, anthracene, rhodamine, 1,8-naphthalimide, coumarin and fluorescein [29–36]. However, some of them have disadvantages like complicated synthetic routes, poor water solubility and being unsuitable for biological application. Thus, there is still a need to further exploit new fluorescent chemosensors for sensing ClO^- in vitro as well as in biological systems [37–39].

Acridine and its derivatives have been interesting subjects to researchers for a long time because of their ability to bind DNA and act as a good fluorophore [40–44]. In addition, benzhydryl isothiocyanate is water-soluble and used for a linker [45]. Therefore, we linked acridine moiety with benzhydryl

isothiocyanate to develop a sensor having the unique photophysical, water-soluble and biocompatible properties for the detection of ClO^- .

Herein, we represent a novel acridine-based fluorescent probe, **BK**, for detecting ClO^- . The reaction of **BK** with ClO^- showed a fluorescent quenching in aqueous media. The sensing ability of the probe was investigated by fluorescent and UV-visible titrations. The sensing mechanism of **BK** towards ClO^- was also demonstrated via ESI-mass spectrometry and theoretical calculations. In addition, the **BK** probe was satisfactorily examined to monitor ClO^- in environmental water samples and zebrafish.

2. Experiments

2.1. Materials and Equipment

All reagents and solvents were purchased from Sigma-Aldrich. ^{13}C NMR (100 MHz) and ^1H NMR (400 MHz) data were provided on a Varian spectrometer. UV-vis and fluorescence measurements were performed on Perkin Elmer UV/Vis and fluorescence spectrometers. ESI-mass data were obtained by a single-quadrupole liquid chromatography detector (ACQUITY QDa).

2.2. Synthesis of KT (*N*-benzhydryl-2-formylhydrazine-1-carbothioamide)

An amount of 2 mmol of formic hydrazide and 2 mmol of benzhydryl isothiocyanate were dissolved in 5 mL of EtOH. The mixture was stirred until a white-colored powder was gained. The resultant powder was filtered and washed with ether. ^1H NMR (deuterated DMSO, 400 MHz) δ (ppm): 11.4 (s, 2H), 10.7 (m, 2H), 8.35 (m, 4H), 8.25 (t, 2H), 8.15 (s, 2H), 8.05 (d, 2H), 7.95 (t, 1H).

2.3. Synthesis of Sensor BK

((E)-N''-(acridine-9-yl)-N'-((benzhydrylamino)(oxo-l4-sulfanylidene)methyl)formimidohydrazide)

An amount of 1 mmol of **KT** and 1 mmol of 9-aminoacridine (**ACR**) were dissolved in 5 mL ethanol. After the solution was stirred at 23 °C overnight, the yellowish powder was filtered and washed with methanol and ether. ^1H NMR in $\text{DMSO}-d_6$, δ : 8.51 (s, 1H), 8.43 (s, 1H), 8.39 (s, 1H), 7.8 (d, 2H, $J = 8.8$ Hz), 7.65 (t, 2H), 7.5 (m, 10H), 7.3 (m, 5H), 7.2 (s, 1H). ^{13}C NMR: $\delta = 142.90, 140.87, 138.05, 132.82, 128.90, 128.26, 128.21, 128.02, 127.73, 124.05, 123.51, 122.71, 112.19, 61.93, 61.05$ ppm. ESI-Mass: m/z calcd for $[\text{C}_{28}\text{H}_{23}\text{N}_5\text{S} - \text{H}^+ + 2 \text{Na}^+ + 2 \text{Cl}^-]^-$: 576.08 found, 575.92.

2.4. General Procedure for the Spectroscopic Studies

Probe **BK** stock solution (1 mM) was prepared in DMF. ClO^- stock solution was prepared by diluting NaClO (500 μmol , 12%, dissolved in H_2O) in distilled water to make 100 mM. All anion and ROS stock solutions (1.0×10^{-1} M) were prepared in bis-tris buffer. The fluorescence and UV-vis data were measured in near 100% aqueous solution (bis-tris, 1×10^{-2} M, pH 7.0).

2.5. Calculation of Quantum Yield

Quantum yield (Φ) was calculated by using quinine as a standard fluorophore (Φ_{F} : 0.54 in 0.1 M H_2SO_4). Equation for quantum yield is:

$$\Phi_{\text{F}}(X) = \Phi_{\text{F}}(S) \left(\frac{A_{\text{S}} F_{\text{X}} / A_{\text{X}} F_{\text{S}}}{n_{\text{X}} / n_{\text{S}}} \right)^2$$

($\Phi_{\text{F}}(X)$: fluorescent quantum yield, x : unknown, s : standard, A : absorbance, n : refractive index of the solvent and F : the area of fluorescence emission curve).

2.6. Imaging Experiments in Zebrafish

Zebrafish embryos were cultured under the former conditions [46]. The 6-day-old embryos were incubated in E2 media replenished with 2×10^{-5} M of **BK** for 15 min and rinsed with E2 media to get rid of the remnant **BK**. One was a control group and the other group further treated with 50 μM of

ClO^- for 15 min was prepared and washed with E2 media. Zebrafish were anesthetized by adding ethyl-3-aminobenzoate. The image of zebrafish was achieved by a fluorescence microscope.

2.7. Cytotoxicity in Zebrafish

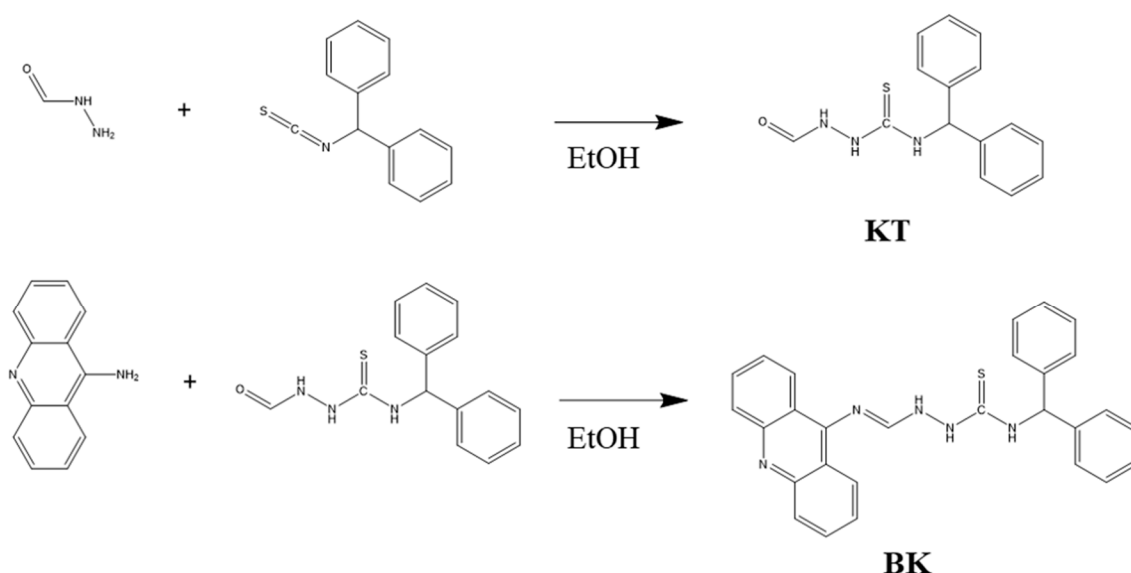
Zebrafish larvae at 6-day old were exposed to 0 and 20 μM of **BK** and 20 μM of 9-aminoacridine in E2 media at 0.05% of DMSO for 20 min. Later they were diverted into 10 $\mu\text{g/mL}$ of AO reagent (Sigma-Aldrich, St. Louis, MO, USA) in E2 media for 60 min. After the larvae were washed with E2 three times, the prepared larvae were mounted and photographed under a Leica fluorescence microscope (MZ10F, Singapore). Apoptosis was identified as an obvious bright spot.

2.8. Theoretical Calculations

DFT/TDDFT calculations on the basis of the hybrid exchange-correlation functional B3LYP were accomplished with the Gaussian 09 W program [47,48]. The 6-31G basis set was applied for all elements (C, S, N, O and H) [49,50]. Frequency calculations of **BK** and **ACR** (9-aminoacridine) were achieved to prove that the optimized forms displayed local minima, and imaginary frequencies were not observed at all. Cossi and Barone's CPCM was employed to consider solvent effect of water [51,52]. To study the electronic properties of singlet excited states, TD-DFT was conducted for the ground state forms of **BK** and **ACR**. The twenty singlet-singlet excitations were quantitatively analyzed. GaussSum 2.2 was used to analyze the contributions of MOs [53].

3. Results and Discussion

The synthetic route for chemosensor **BK** is outlined in Scheme 1 and it was successfully characterized by ^1H and ^{13}C NMR and ESI-MS. Sensing behavior of **BK** toward ClO^- was investigated by using several analytical tools like UV-visible and fluorescent spectroscopy, ^1H NMR titration, and calculations.



Scheme 1. Synthesis of **BK** ((E)-2-((acridine-9-ylimino)methyl)-N-benzhydrylhydrazine-1-carbothioamide).

3.1. Spectroscopic Investigations of **BK** to ClO^-

Selectivity was one of the essential indicators for measuring capacity of fluorescent probe. Reactivity of **BK** to diverse analytes (N_3^- , Cl^- , H_2O_2 , CN^- , S^{2-} , I^- , tBuOOH , SCN^- , OAc^- , Br^- , AcOOH , H_2PO_4^- , BzO^- , F^- , NO_2^- and ClO^-) in bis-tris buffer (1×10^{-2} M, pH 7.0, Figure 1) was tested to evaluate the selectivity for ClO^- . With excitation at 350 nm, free sensor **BK** displayed a markedly strong fluorescence emission at 455 nm ($\Phi = 0.6659$). Upon addition of each analyte into **BK** solution,

only ClO^- induced the prominent fluorescent decrease ($\Phi = 0.0047$) whereas other analytes did not show any noticeable changes. Therefore, the sensor **BK** could serve as a preeminent fluorescent sensor for ClO^- .

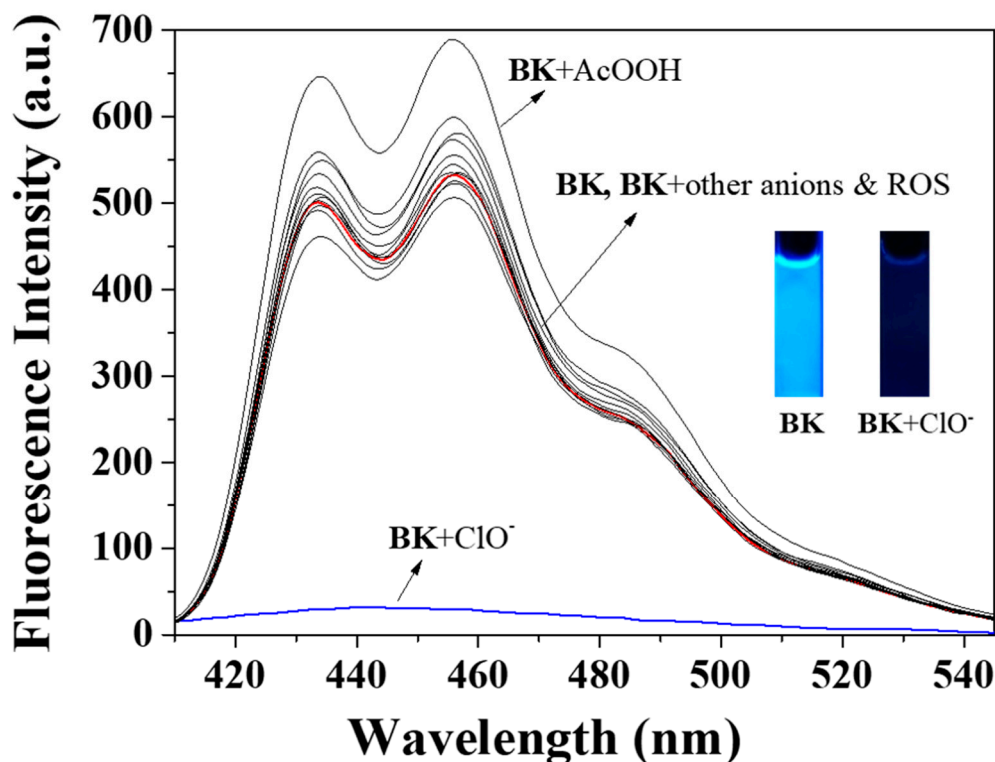


Figure 1. Fluorescence spectra of **BK** (1×10^{-5} M) with varied analytes (220 equiv). ROS: Reactive oxygen species.

To examine the response of **BK** to ClO^- , the spectral titrations were carried out (Figure 2). On the addition of different ClO^- amounts to **BK**, the fluorescence emission of 455 nm constantly decreased and was saturated at 220 equiv. The measured limit of detection ($C_{\text{DL}} = 3\sigma/k$) for ClO^- was $7.65 \mu\text{M}$ (Figure S1 in the Supplementary Materials). The UV-visible titration displayed that the absorbance of 280 nm constantly increased and the bands at 260 nm and 400 nm reduced with an obvious isosbestic point at 370 nm (Figure 3).

To elucidate the detecting mechanism of ClO^- , we conducted the ESI-mass experiment (Figure S2). The peak of 322.08 (m/z) was indicative of $[\text{ACRO} + \text{Cl}^- + \text{MeCN} + 2\text{H}_2\text{O}]^-$ [calcd, 322.10], indicating the cleavage reaction product of **BK** by ClO^- . ^1H NMR titration was carried out to observe the formation of **ACR** (Figure 4). With gradual addition of ClO^- to **BK**, the imine proton H_5 disappeared, and the amine proton H_A of **ACR** and the aldehyde proton H_B of **KT** appeared.

On the other hand, as 9-aminoacridine was highly fluorescent in nature, we examined the interaction of 9-aminoacridine with ClO^- . As shown in Figure S3, ClO^- quenched the fluorescence of 9-aminoacridine, most likely due to an oxidation reaction. These observations led us to propose that the probe **BK** was cleaved by ClO^- via the cleavage process of the $\text{C}=\text{N}$ bond to produce 9-aminoacridine. Then, the fluorescent 9-aminoacridine was subsequently quenched by ClO^- (Scheme 2).

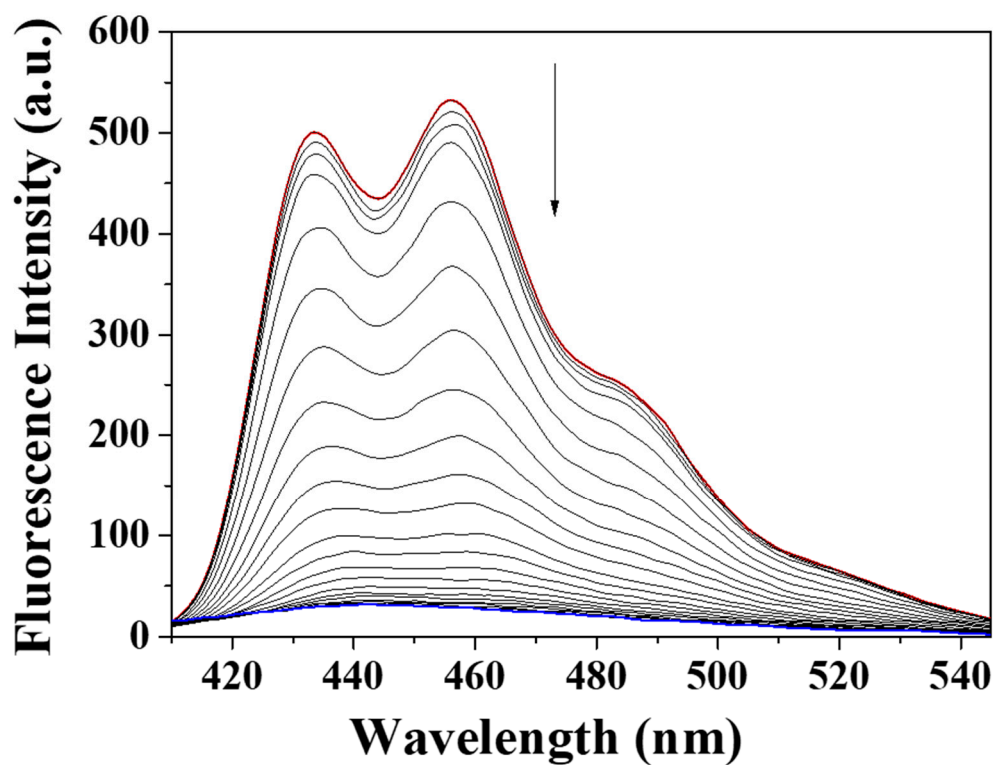


Figure 2. Fluorescent changes of BK (1×10^{-5} M) with different concentrations of ClO⁻.

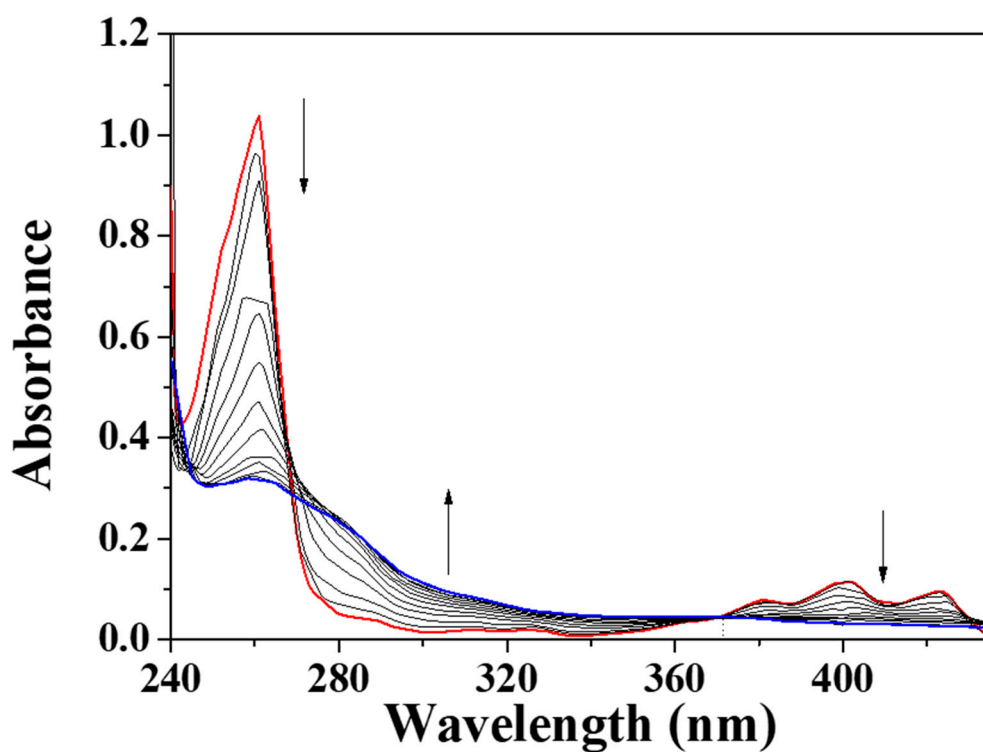


Figure 3. UV-vis variations of probe BK (1×10^{-5} M) with different concentrations of ClO⁻.

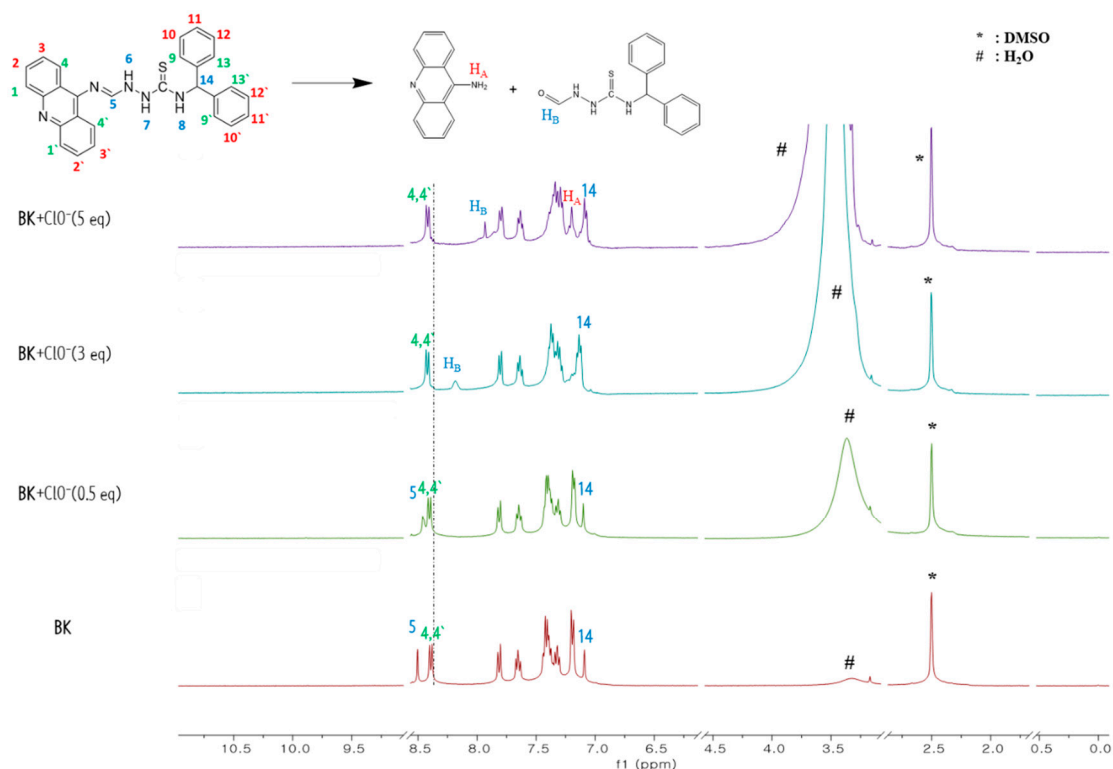
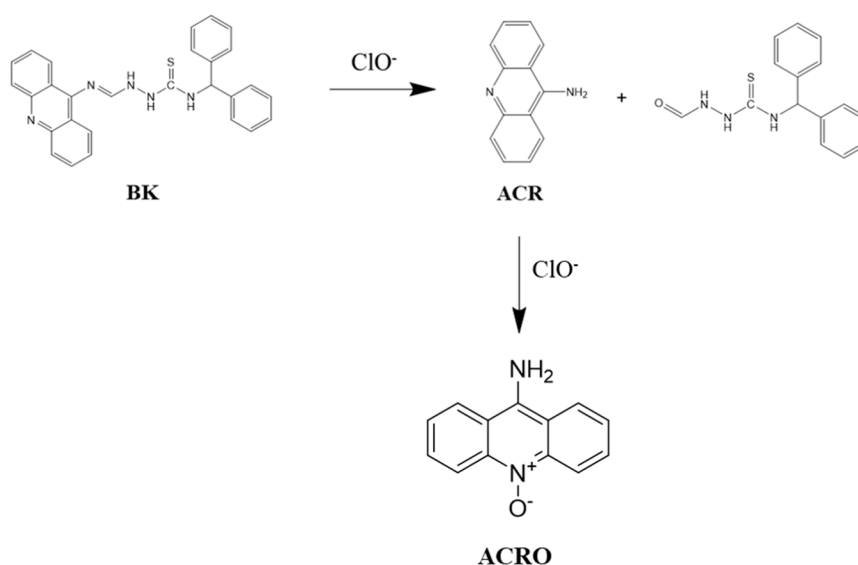


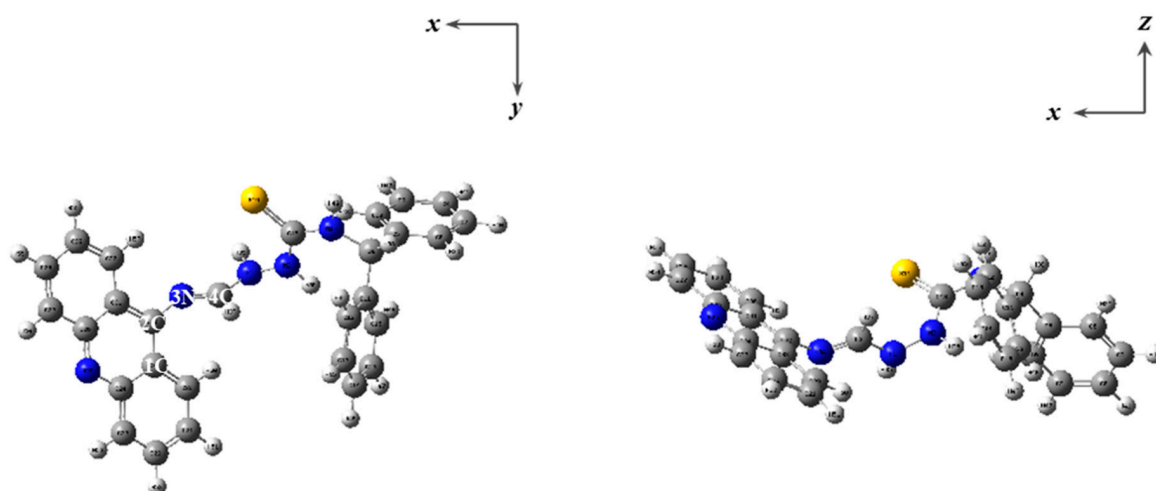
Figure 4. ^1H NMR titration of **BK** with ClO^- .



Scheme 2. Cleavage sensing mechanism of **BK** by ClO^- .

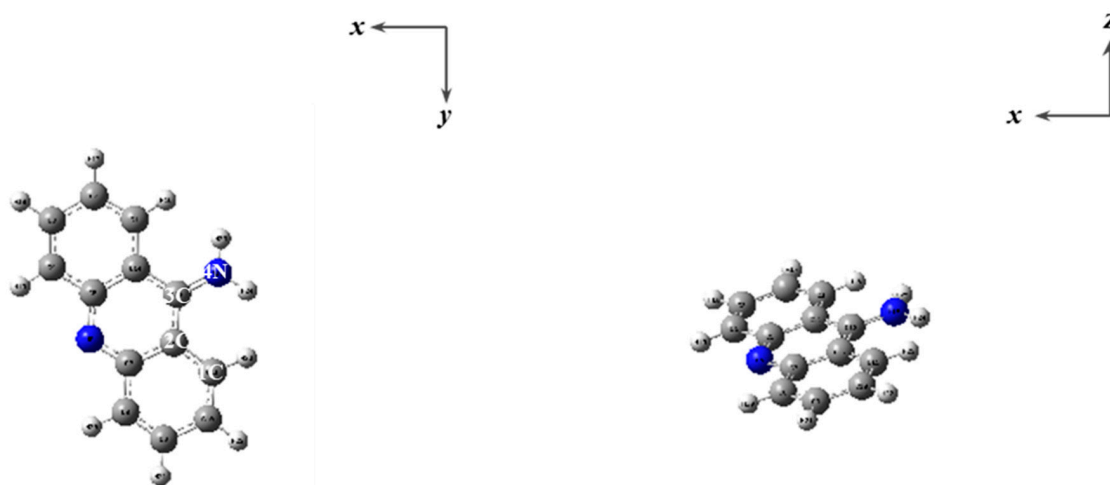
To further comprehend the cleavage sensing mechanism of **BK** by ClO^- , computational calculations were achieved. Energy-optimized forms of **BK** and **ACR** were analyzed with DFT/B3LYP/6-31G (d,p) basis sets (Figure 5). Using the optimized forms of **BK** and **ACR**, TD-DFT calculations were performed for analyzing transition energies and molecular orbitals (Figures S4–S6). The MOs of **BK** at the first lowest excited state were identified as the HOMO \rightarrow LUMO transitions (391.73 nm, Figure S5), which turned out to be $\pi \rightarrow \pi^*$ transitions. For **ACR**, the MOs at the first lowest excited state were identified as the HOMO \rightarrow LUMO (391.84 nm, Figure S6), which turned out to be $\pi \rightarrow \pi^*$ transitions. In addition, the decreased oscillator strength of **ACR** was corresponded with the decreased UV-vis absorbance.

These outcomes drove us to elucidate that fluorescent sensor **BK** was quenched due to the cleavage of the C=N bond.



Dihedral angle = 1C, 2C, 3N, 4C : -66.21°

(a)



Dihedral angle = 1C, 2C, 3C, 4N : 0.00°

(b)

Figure 5. Energy-minimized forms of (a) BK and (b) 9-aminoacridine (ACR).

Another vital indicator in the sensing process is the ability of the fluorescent probe not to be disturbed by the competitive analytes. When **BK** was exposed with both ClO^- and diverse analytes (N_3^- , Cl^- , H_2O_2 , tBuOOH , OAc^- , Br^- , AcOOH , H_2PO_4^- , BzO^- , F^- and NO_2^-), the guest analytes did not hinder the sensing of ClO^- (Figure 6). Only, the presence of tBuOOH and OAc^- showed slight interference in determining ClO^- . CN^- , S^{2-} , I^- and SCN^- were excluded from the competition because they reacted directly with ClO^- .

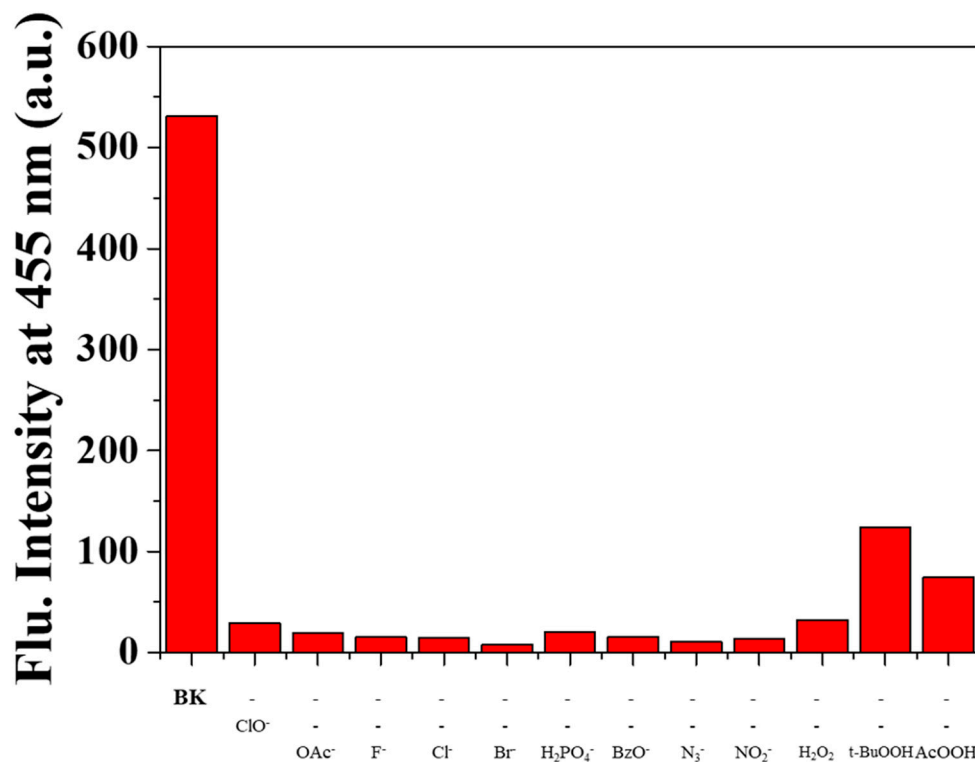


Figure 6. Competitive selectivity of **BK** (1×10^{-5} M) to ClO^- (220 equiv) with other analytes (220 equiv).

The pH was a vital condition related with physiological processes and even cellular behaviors. Thus, we checked the effect of pH on sensing property of **BK** for ClO^- at pH ranging from six to nine (Figure 7). **BK** displayed significant fluorescence intensity at the pH range of six to nine. The intensity of **BK** treated with ClO^- was completely quenched at pH six to nine. These observations indicated that **BK** could be applicable as a probe for detecting ClO^- at pH six to nine.

To explore practical utility of **BK**, the application of **BK** in real samples was accomplished in both tap and drinking water samples. The reliable R.S.D. values and recoveries demonstrated that sensor **BK** had a valuable potential for being used as a dependable tool to monitor ClO^- in real water samples (Table 1).

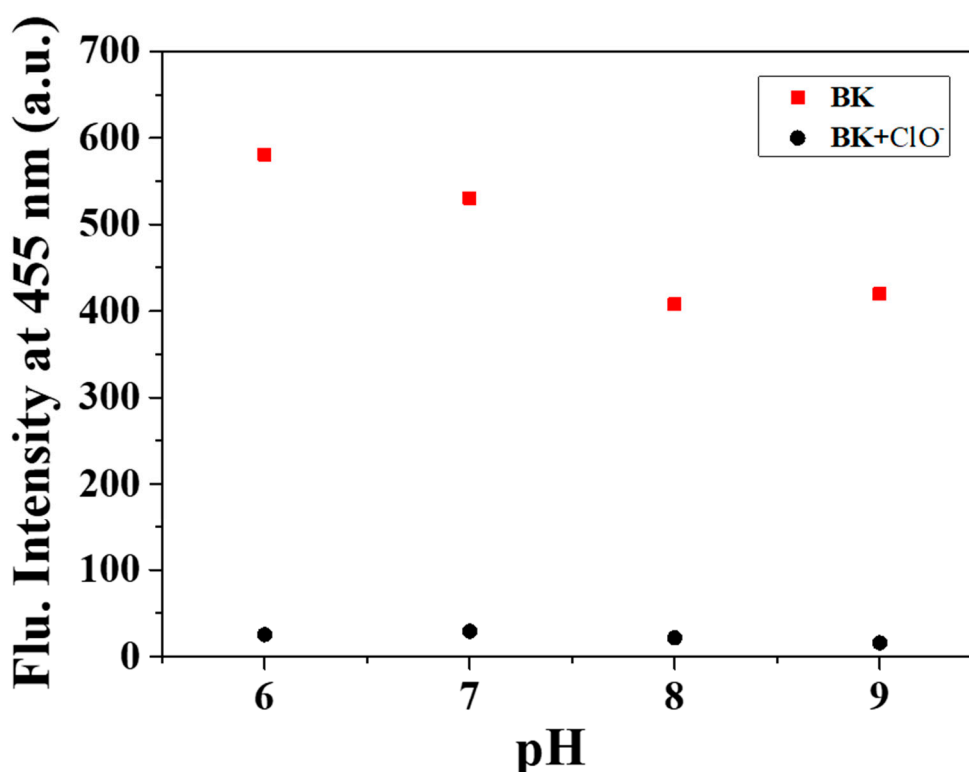


Figure 7. Fluorescence intensity (at 455 nm) of **BK** with ClO^- at pH values from six to nine.

Table 1. Determination of ClO^- .^a

Sample.	ClO^- Added (μM)	ClO^- Found (μM)	Recovery (%)	R.S.D. (n = 3) (%)
Drinking water	0.00	0.00		
	60.00 ^b	62.88	104.80	0.32
Tap water	0.00	0.00		
	60.00 ^b	62.16	103.60	0.41

^a Conditions: [**BK**] = 10 μM in bis-tris buffer. ^b 60.00 μM of ClO^- was artificially added.

3.2. In Vivo Imaging in Zebrafish

To test whether the probe **BK** is applicable under biological conditions, zebrafish were incubated with **BK** (20 μM) and sequentially treated with two different concentrations of ClO^- (0 and 50 μM) for imaging (Figure 8). Zebrafish incubated with **BK** exhibited a green fluorescence image, but the green fluorescence was eliminated in the presence of ClO^- . Meanwhile, the cytotoxicity test of **BK** was examined by AO staining (Figure S7). The AO stained results showed that no apoptosis was observed in control and the presence of **BK** and 9-aminoacridine. Zebrafish experiments proved that **BK** was organism-permeable and can monitor ClO^- in living organisms. Importantly, **BK** is the first fluorescent turn-off sensor capable of sensing ClO^- in zebrafish (Table S1) [1,38,54–59].

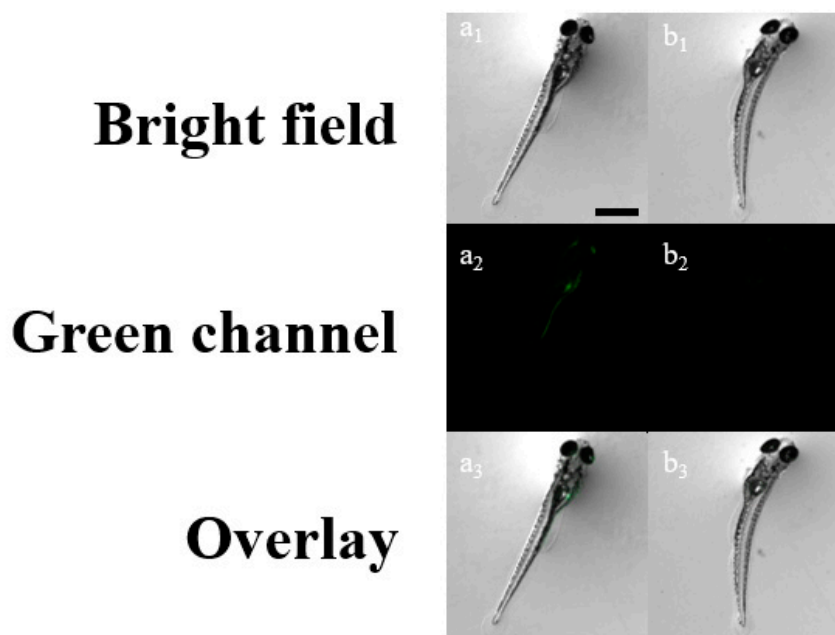


Figure 8. Fluorescence images of zebrafish treated with **BK** followed by addition of ClO^- ($\lambda_{\text{ex}} = 502$ nm and $\lambda_{\text{em}} = 526$ nm). (**a**₁–**a**₃): **BK** only; (**b**₁–**b**₃): **BK** with 5×10^{-5} M ClO^- . [**BK**] = 2×10^{-5} M. Scale bar: 0.89 mm.

4. Conclusions

We have synthesized an acridine-based chemosensor for monitoring ClO^- in a near-perfect aqueous media. Probe **BK** selectively detected ClO^- over other relevant species including ROS, and its intense blue fluorescence was notably quenched with the addition of ClO^- . The detection limit of **BK** for ClO^- was analyzed to be $7.65 \mu\text{M}$. **BK** was employed for quantitative measurement of ClO^- in real water samples and zebrafish. Significantly, **BK** is the first fluorescent turn-off sensor capable of sensing ClO^- in zebrafish to date. The promising outcomes indicate that **BK** can serve as a potential chemosensor for monitoring ClO^- in chemical, environmental and biological systems. We believe that these results will be merited for further development of ClO^- sensors.

Supplementary Materials: The following are available online at <http://www.mdpi.com/1424-8220/20/17/4764/s1>, Table S1: Examples of fluorescent chemosensors for detecting ClO^- in zebrafish, Figure S1: Determination of the detection limit for ClO^- by **BK** ($10 \mu\text{M}$) based on the fluorescence emission at 455 nm; Figure S2: Negative-ion electrospray ionization mass spectrum of **BK** ($10 \mu\text{M}$) upon addition of NaClO (200 equiv); Figure S3: Molecular orbital diagrams and excitation energies of (a) **BK** and (b) **ACR**; Figure S4: (a) The theoretical excitation energies and the experimental UV-vis spectrum of **BK**. (b) The major electronic transition energies and molecular orbital contributions for **BK** (H = HOMO and L = LUMO); Figure S5: (a) The theoretical excitation energies and the experimental UV-vis spectrum of **ACR**. (b) The major electronic transition energies and molecular orbital contributions for **ACR** (H = HOMO and L = LUMO); Figure S6: (a) The theoretical excitation energies and the experimental UV-vis spectrum of **ACR**. (b) The major electronic transition energies and molecular orbital contributions for **ACR** (H = HOMO and L = LUMO); Figure S7. AO-stained zebrafish exposed to (a) $0 \mu\text{M}$ and (b) $20 \mu\text{M}$ of **BK** and (c) $20 \mu\text{M}$ of 9-aminoacridine.

Author Contributions: S.C.L. and C.K. provided the initial idea for this work; S.C.L., S.P. and H.S. contributed to the collection and analysis of field test data; K.-T.K. and G.L. contributed to the analyses of results; S.C.L. and C.K. wrote the paper. All authors have read and agreed to the published version of the manuscript.

Funding: This research received no external funding.

Acknowledgments: KEITI (Korea Environment Industry and Technology Institute) (2016001970001) are kindly acknowledged.

Conflicts of Interest: The authors declare no conflict of interest.

References

1. He, X.; Xu, C.; Xiong, W.; Qian, Y.; Fan, J.; Ding, F.; Deng, H.; Chen, H.; Shen, J. The ICT-based fluorescence and colorimetric dual sensing of endogenous hypochlorite in living cells, bacteria, and zebrafish. *Analyst* **2020**, *145*, 29–33. [[CrossRef](#)]
2. Kang, J.; Huo, F.; Zhang, Y.; Chao, J.; Strongin, R.M.; Yin, C. Detecting intracellular ClO^- with ratiometric fluorescent signal and its application in vivo. *Sens. Actuators B Chem.* **2018**, *273*, 1532–1538. [[CrossRef](#)]
3. Huo, B.; Du, M.; Shen, A.; Li, M.; Lai, Y.; Bai, X.; Gong, A.; Fang, L.; Yang, Y. A “light-up” fluorescent probe based on TEMPO-oxidation for the detection of ClO^- and application in real samples. *Sens. Actuators B Chem.* **2019**, *284*, 23–29. [[CrossRef](#)]
4. Kettle, A.J.; Albrett, A.M.; Chapman, A.L.; Dickerhof, N.; Forbes, L.V.; Khalilova, I.; Turner, R. Measuring chlorine bleach in biology and medicine. *Biochim. Biophys. Acta Gen. Subj.* **2014**, *1840*, 781–793. [[CrossRef](#)]
5. Zhang, Y.R.; Liu, Y.; Feng, X.; Zhao, B.X. Recent progress in the development of fluorescent probes for the detection of hypochlorous acid. *Sens. Actuators B Chem.* **2017**, *240*, 18–36. [[CrossRef](#)]
6. Reja, S.I.; Bhalla, V.; Sharma, A.; Kaur, G.; Kumar, M. A highly selective fluorescent probe for hypochlorite and its endogenous imaging in living cells. *Chem. Commun.* **2014**, *50*, 11911–11914. [[CrossRef](#)] [[PubMed](#)]
7. Wang, L.; Hu, Y.; Qu, Y.; Xu, J.; Cao, J. Aggregated-induced emission phenothiazine probe for selective ratiometric response of hypochlorite over other reactive oxygen species. *Dye. Pigment.* **2016**, *128*, 54–59. [[CrossRef](#)]
8. Shim, M.S.; Xia, Y. A reactive oxygen species (ROS)-responsive polymer for safe, efficient, and targeted gene delivery in cancer cells. *Angew. Chem. Int. Ed.* **2013**, *52*, 6926–6929. [[CrossRef](#)]
9. Yang, Y.; Yin, C.; Huo, F.; Chao, J.; Zhang, Y.; Jin, S. Simple 1,8-diaminonaphthalene-based fluorescence chemosensor for hypochlorites and its practical application. *Sens. Actuators B Chem.* **2014**, *199*, 226–231. [[CrossRef](#)]
10. Huang, Y.; Zhang, Y.; Huo, F.; Chao, J.; Yin, C. A near-infrared ratiometric fluorescent probe with large Stokes based on isophorone for rapid detection of ClO^- and its bioimaging in cell and mice. *Sens. Actuators B Chem.* **2019**, *287*, 453–458. [[CrossRef](#)]
11. Jiang, Y.; Wu, S.; Jin, C.; Wang, B.; Shen, J. Novel diaminomaleonitrile-based fluorescent probe for ratiometric detection and bioimaging of hypochlorite. *Sens. Actuators B Chem.* **2018**, *265*, 365–370. [[CrossRef](#)]
12. Huo, F.J.; Zhang, J.J.; Yang, Y.T.; Chao, J.B.; Yin, C.X.; Zhang, Y.B.; Chen, T.G. A fluorescein-based highly specific colorimetric and fluorescent probe for hypochlorites in aqueous solution and its application in tap water. *Sens. Actuators B Chem.* **2012**, *166*, 44–49. [[CrossRef](#)]
13. Lv, J.; Chen, Y.; Wang, F.; Wei, T.; Zhang, Z.; Qiang, J.; Chen, X. A mitochondria-targeted fluorescent probe based on fluorescein derivative for detection of hypochlorite in living cells. *Dye. Pigment.* **2018**, *148*, 353–358. [[CrossRef](#)]
14. Du, J.; Hu, M.; Fan, J.; Peng, X. Fluorescent chemodosimeters using “mild” chemical events for the detection of small anions and cations in biological and environmental media. *Chem. Soc. Rev.* **2012**, *41*, 4511–4535. [[CrossRef](#)] [[PubMed](#)]
15. Lee, S.C.; Kim, C. Naphthol-naphthalimide based ‘turn-on’ fluorescent sensor for ClO^- in aqueous media and test kit. *Inorg. Chem. Commun.* **2019**, *108*, 107545. [[CrossRef](#)]
16. Sam, C.H.; Lu, H.K. The role of hypochlorous acid as one of the reactive oxygen species in periodontal disease. *J. Dent. Sci.* **2009**, *4*, 45–54. [[CrossRef](#)]
17. Steinbeck, M.J.; Nesti, L.J.; Sharkey, P.F.; Parvizi, J. Myeloperoxidase and chlorinated peptides in osteoarthritis: Potential biomarkers of the disease. *J. Orthop. Res.* **2007**, *25*, 1128–1135. [[CrossRef](#)]
18. Pattison, D.I.; Davies, M.J. Evidence for rapid inter- and intramolecular chlorine transfer reactions of histamine and carnosine chloramines: Implications for the prevention of hypochlorous-acid-mediated damage. *Biochemistry* **2006**, *45*, 8152–8162. [[CrossRef](#)]
19. Tian, F.; Jia, Y.; Zhang, Y.; Song, W.; Zhao, G.; Qu, Z.; Li, C.; Chen, Y.; Li, P. A HClO-specific near-infrared fluorescent probe for determination of Myeloperoxidase activity and imaging mitochondrial HClO in living cells. *Biosens. Bioelectron.* **2016**, *86*, 68–74. [[CrossRef](#)]
20. Song, X.; Dong, B.; Kong, X.; Wang, C.; Zhang, N.; Lin, W. Construction of a ratiometric fluorescent probe with an extremely large emission shift for imaging hypochlorite in living cells. *Spectrochim. Acta Part A Mol. Biomol. Spectrosc.* **2018**, *188*, 394–399. [[CrossRef](#)]

21. Jin, L.; Xu, M.; Jiang, H.; Wang, W.; Wang, Q. A simple fluorescein derived colorimetric and fluorescent “off-on” sensor for the detection of hypochlorite. *Anal. Methods* **2018**, *10*, 4562–4569. [[CrossRef](#)]
22. Zhang, P.; Wang, H.; Hong, Y.; Yu, M.; Zeng, R.; Long, Y.; Chen, J. Selective visualization of endogenous hypochlorous acid in zebrafish during lipopolysaccharide-induced acute liver injury using a polymer micelles-based ratiometric fluorescent probe. *Biosens. Bioelectron.* **2018**, *99*, 318–324. [[CrossRef](#)] [[PubMed](#)]
23. Adegoke, O.; Forbes, P.B.C. Challenges and advances in quantum dot fluorescent probes to detect reactive oxygen and nitrogen species: A review. *Anal. Chim. Acta* **2015**, *862*, 1–13. [[CrossRef](#)] [[PubMed](#)]
24. Jiao, X.; Liu, C.; Wang, Q.; Huang, K.; He, S.; Zhao, L.; Zeng, X. Fluorescence probe for hypochlorous acid in water and its applications for highly lysosome-targetable live cell imaging. *Anal. Chim. Acta* **2017**, *969*, 49–56. [[CrossRef](#)] [[PubMed](#)]
25. Goswami, S.; Paul, S.; Manna, A. Carbazole based hemicyanine dye for both “naked eye” and ‘NIR’ fluorescence detection of CN^- in aqueous solution: From molecules to low cost devices (TLC plate sticks). *Dalton Trans.* **2013**, *42*, 10682–10686. [[CrossRef](#)]
26. Goswami, S.; Manna, A.; Paul, S.; Quah, C.K.; Fun, H.K. Rapid and ratiometric detection of hypochlorite with real application in tap water: Molecules to low cost devices (TLC sticks). *Chem. Commun.* **2013**, *49*, 11656–11658. [[CrossRef](#)]
27. Kim, H.N.; Lee, M.H.; Kim, H.J.; Kim, J.S.; Yoon, J. A new trend in rhodamine-based chemosensors: Application of spirolactam ring-opening to sensing ions. *Chem. Soc. Rev.* **2008**, *37*, 1465–1472. [[CrossRef](#)]
28. Chen, X.; Baek, K.H.; Kim, Y.; Kim, S.J.; Shin, I.; Yoon, J. A selenolactone-based fluorescent chemodosimeter to monitor mercury/methylmercury species in vitro and in vivo. *Tetrahedron* **2010**, *66*, 4016–4021. [[CrossRef](#)]
29. Wang, X.; Song, F.; Peng, X. A versatile fluorescent probe for imaging viscosity and hypochlorite in living cells. *Dye. Pigment.* **2016**, *125*, 89–94. [[CrossRef](#)]
30. Lou, X.; Zhang, Y.; Li, Q.; Qin, J.; Li, Z. A highly specific rhodamine-based colorimetric probe for hypochlorites: A new sensing strategy and real application in tap water. *Chem. Commun.* **2011**, *47*, 3189–3191. [[CrossRef](#)]
31. Long, L.; Zhang, D.; Li, X.; Zhang, J.; Zhang, C.; Zhou, L. A fluorescence ratiometric sensor for hypochlorite based on a novel dual-fluorophore response approach. *Anal. Chim. Acta* **2013**, *775*, 100–105. [[CrossRef](#)] [[PubMed](#)]
32. Maity, D.; Karthigeyan, D.; Kundu, T.K.; Govindaraju, T. FRET-based rational strategy for ratiometric detection of Cu^{2+} and live cell imaging. *Sens. Actuators B Chem.* **2013**, *176*, 831–837. [[CrossRef](#)]
33. Hwang, S.M.; Chae, J.B.; Kim, C. A Phenanthroimidazole-based Fluorescent Turn-Off Chemosensor for the Selective Detection of Cu^{2+} in Aqueous Media. *Bull. Korean Chem. Soc.* **2018**, *39*, 925–930. [[CrossRef](#)]
34. Koide, Y.; Urano, Y.; Hanaoka, K.; Terai, T.; Nagano, T. Development of an Si-rhodamine-based far-red to near-infrared fluorescence probe selective for hypochlorous acid and its applications for biological imaging. *J. Am. Chem. Soc.* **2011**, *133*, 5680–5682. [[CrossRef](#)]
35. Shiraiishi, Y.; Yamada, C.; Hirai, T. A coumarin-dihydroperimidine dye as a fluorescent chemosensor for hypochlorite in 99% water. *RSC Adv.* **2019**, *9*, 28636–28641. [[CrossRef](#)]
36. Grabchev, I.; Petkov, C.; Bojinov, V. 1,8-Naphthalimides as blue emitting fluorophores for polymer materials. *Macromol. Mater. Eng.* **2002**, *287*, 904–908. [[CrossRef](#)]
37. Liu, Y.; Zhao, C.; Zhao, X.; Liu, H.; Wang, Y.; Du, Y.; Wei, D. A selective N,N-dithenoyl-rhodamine based fluorescent probe for Fe^{3+} detection in aqueous and living cells. *J. Environ. Sci.* **2020**, *90*, 180–188. [[CrossRef](#)]
38. He, X.; Chen, H.; Xu, C.; Fan, J.; Xu, W.; Li, Y.; Deng, H.; Shen, J. Ratiometric and colorimetric fluorescent probe for hypochlorite monitor and application for bioimaging in living cells, bacteria and zebrafish. *J. Hazard. Mater.* **2020**, *388*, 122029. [[CrossRef](#)]
39. Wang, Y.; He, J.; Zheng, M.; Qin, M.; Wei, W. Dual-emission of Eu based metal-organic frameworks hybrids with carbon dots for ratiometric fluorescent detection of Cr (VI). *Talanta* **2019**, *191*, 519–525. [[CrossRef](#)]
40. Wang, C.; Fu, J.; Yao, K.; Xue, K.; Xu, K.; Pang, X. Acridine-based fluorescence chemosensors for selective sensing of Fe^{3+} and Ni^{2+} ions. *Spectrochim. Acta Part A Mol. Biomol. Spectrosc.* **2018**, *199*, 403–411. [[CrossRef](#)]
41. Nunes, M.C.; dos Santos Carlos, F.; Fuganti, O.; Galindo, D.D.M.; De Boni, L.; Abate, G.; Nunes, F.S. Turn-on fluorescence study of a highly selective acridine-based chemosensor for Zn^{2+} in aqueous solutions. *Inorg. Chim. Acta* **2020**, *499*, 119191. [[CrossRef](#)]
42. Wang, C.; Wang, P.; Liu, X.; Fu, J.; Xue, K.; Xu, K. Novel enantioselective fluorescent sensors for tartrate anion based on acridinezswsxa. *Luminescence* **2017**, *32*, 1313–1318. [[CrossRef](#)] [[PubMed](#)]

43. Janovec, L.; Kožurková, M.; Sabolová, D.; Ungvarský, J.; Paulíková, H.; Plšíková, J.; Vantová, Z.; Imrich, J. Cytotoxic 3,6-bis((imidazolidinone)imino)acridines: Synthesis, DNA binding and molecular modeling. *Bioorganic Med. Chem.* **2011**, *19*, 1790–1801. [[CrossRef](#)] [[PubMed](#)]
44. Dai, Y.; Xu, K.; Li, Q.; Wang, C.; Liu, X.; Wang, P. Acridine-based complex as amino acid anion fluorescent sensor in aqueous solution. *Spectrochim. Acta Part A Mol. Biomol. Spectrosc.* **2016**, *157*, 1–5. [[CrossRef](#)]
45. Kim, A.; Kim, C. A hydrazono-quinoline-based chemosensor sensing In^{3+} and Zn^{2+} via fluorescence turn-on and ClO^- via color change in aqueous solution. *New J. Chem.* **2019**, *43*, 7320–7328. [[CrossRef](#)]
46. Jung, J.M.; Lee, S.Y.; Nam, E.; Lim, M.H.; Kim, C. A highly selective turn-on chemosensor for Zn^{2+} in aqueous media and living cells. *Sens. Actuators B Chem.* **2017**, *244*, 1045–1053. [[CrossRef](#)]
47. Becke, A.D. Density-functional thermochemistry. III. The role of exact exchange. *J. Chem. Phys.* **1993**, *98*, 5648–5652. [[CrossRef](#)]
48. Lee, C.; Yang, W.; Parr, R.G. Development of the Colle-Salvetti correlation-energy formula into a functional of the electron density. *Phys. Rev. B* **1988**, *37*, 785. [[CrossRef](#)]
49. Hariharan, P.C.; Pople, J.A. The influence of polarization functions on molecular orbital hydrogenation energies. *Chim. Acta* **1973**, *28*, 213–222. [[CrossRef](#)]
50. Gordon, M.S.; Binkley, J.S.; Pople, J.A.; Pietro, W.J.; Hehre, W.J. Self-Consistent Molecular-Orbital Methods. 22. Small Split-Valence Basis Sets for Second-Row Elements. *J. Am. Chem. Soc.* **1982**, *104*, 2797–2803. [[CrossRef](#)]
51. Barone, V.; Cossi, M. Quantum calculation of molecular energies and energy gradients in solution by a conductor solvent model. *J. Phys. Chem. A* **1998**, *102*, 1995–2001. [[CrossRef](#)]
52. Cossi, M.; Barone, V. Time-dependent density functional theory for molecules in liquid solutions. *J. Chem. Phys.* **2001**, *115*, 4708. [[CrossRef](#)]
53. O'boyle, N.M.; Tenderholt, A.L.; Langner, K.M. Cclib: A library for package-independent computational chemistry algorithms. *J. Comput. Chem.* **2008**, *29*, 839–845. [[CrossRef](#)] [[PubMed](#)]
54. Chen, H.; Sun, T.; Qiao, X.G.; Tang, Q.O.; Zhao, S.C.; Zhou, Z. Red-emitting fluorescent probe for detecting hypochlorite acid in vitro and in vivo. *Spectrochim. Acta Part A Mol. Biomol. Spectrosc.* **2018**, *204*, 196–202. [[CrossRef](#)] [[PubMed](#)]
55. Lan, J.; Guo, J.; Jiang, X.; Chen, Y.; Hu, Z.; Que, Y.; Li, H.; Gu, J.; Ho, R.J.Y.; Zeng, R.; et al. A new dicyanoisophorone-based ratiometric and colorimetric near-infrared fluorescent probe for specifically detecting hypochlorite and its bioimaging on a model of acute inflammation. *Anal. Chim. Acta* **2020**, *1094*, 70–79. [[CrossRef](#)] [[PubMed](#)]
56. Duan, C.; Won, M.; Verwilt, P.; Xu, J.; Kim, H.S.; Zeng, L.; Kim, J.S. In vivo imaging of endogenously produced HClO in zebrafish and mice using a bright, photostable ratiometric fluorescent probe. *Anal. Chem.* **2019**, *91*, 4172–4178. [[CrossRef](#)]
57. Wang, N.; Xu, W.; Song, D.; Ma, P. A fluorescein-carbazole-based fluorescent probe for imaging of endogenous hypochlorite in living cells and zebrafish. *Spectrochim. Acta Part A Mol. Biomol. Spectrosc.* **2020**, *227*, 117692. [[CrossRef](#)]
58. So, H.; Cho, H.; Lee, H.; Tran, M.C.; Kim, K.T.; Kim, C. Detection of zinc (II) and hypochlorite by a thiourea-based chemosensor via two emission channels and its application in vivo. *Microchem. J.* **2020**, *155*, 104788. [[CrossRef](#)]
59. Liu, C.; Li, Z.; Yu, C.; Chen, Y.; Liu, D.; Zhuang, Z.; Jia, P.; Zhu, H.; Zhang, X.; Yu, Y.; et al. Development of a Concise Rhodamine-Formylhydrazine Type Fluorescent Probe for Highly Specific and Ultrasensitive Tracing of Basal HOCl in Live Cells and Zebrafish. *ACS Sens.* **2019**, *4*, 2156–2163. [[CrossRef](#)]

